Design of Dielectric Electroactive Polymers for a Compact and Scalable Variable Stiffness Device

Sanjay Dastoor and Mark Cutkosky

***Abstract*— We present the design, analysis, and experimental validation of a variable stiffness device based on annular dielectric electroactive polymer (EAP) actuators. The device is based on a diaphragm geometry, which partially linearizes the viscoelastic response of acrylic dielectrics, providing voltage-controlled stiffness without high damping losses. Multiple diaphragms can be connected in a single device to increase stiffness or provide custom stiffness profiles. The geometry is analyzed to determine the relationship among force, displacement and voltage. A single-layer diaphragm was constructed and tested to validate the concept, demonstrating up to 10x change in stiffness.**

I. Introduction

A. Motivation

Passive compliance has become an increasingly important aspect of robotic and rehabilitation systems. Classically, robots have relied on stiff appendages and precise position control of joints to facilitate high-speed trajectory tracking. However, many applications benefit from an alternative approach that relies on inherent compliance to improve performance.

Biologically-inspired robots have long included passive compliance as a key design element. Running [1], hopping [2], climbing [3] and perching [4] robots have been designed where appropriate selection of joint and appendage impedance leads to reduced shock forces, increased robustness, and increased efficency via energy storage and release. Such strategies are inspired in part by animals' ability to vary joint impedance via co-contraction of antagonistic muscles [5]. Active impedance control with stiff actuators is possible, but is limited by bandwidth, weight, and power consumption.

Human-safe robot operation also shares similar requirements. In industrial robot manipulators [6], passive compliance helps prevent humans from experiencing high forces during accidental contact. In rehabilitation devices [7], impedance matching with the patient is necessary for many tasks. Here, passive compliance promotes "fail-safe" operation when compared to active impedance control.

B. Previous Work

Passive compliance can be achieved through devices such as the series elastic actuator (SEA), combining a passive spring and a stiff motor [8]. Advantages include low weight and few moving parts. However, their ability to vary this compliance is still limited to active control of the serial motor. To achieve variable passive compliance, several different techniques can be used, broadly categorized into antagonistic systems and structure-controlled systems [9].

Antagonistic systems rely on manipulation of nonlinear springs to change their equilibrium position. An example such as AMASC [10] can independently control joint position and stiffness. These systems, while similar to the biological strategy of muscle co-contraction, have disadvantages in compact robotic devices due to their motor size requirements, power usage, mechanical complexity, and weight.

Structure-controlled systems exploit a change in passive spring geometry or coupling. Varying the effective length of a spring [11][12] or the moment of inertia of a beam [13] are common methods to achieve this. While they use less power to change stiffness and are much simpler mechanically, these systems still have moving parts and often a heavy or bulky actuator, precluding their use in applications with tight mass or volume constraints.

C. Electroactive Polymers

Electroactive polymers have been described as "artificial muscles" due to several muscle-like properties, such as inherent passive compliance and damping, low weight, flexible geometry, and silent operation. They have been examined most often as a prime mover actuator, with very high strains and forces possible using careful design and multiple film layers [14]. However, their disadvantages include high voltage requirements, low bandwidth due to hysteretic losses, and actuator failure due to manufacturing defects, mechanical film overstrain and tearing, and dielectric breakdown and shorting.

Their use as a tunable impedance device was first suggested through electrical loading or active feedback control by Pelrine [15], who later demonstrated stiffness changes up to 10x due to film buckling in a planar actuator geometry [16]. Variable damping properties through an external control circuit have also been demonstrated [17].

In this paper, we introduce a variable stiffness device that utilizes the applied voltage (from 0 to 6 kV at 100 μA) to vary the effective mechanical pre-strain of the actuator film, allowing a 7x to 10x change in stiffness. The geometry and construction of the device greatly reduce failure rates, linearize the viscoelastic hysteresis of the film material, and allow scaling to a range of displacements and forces suited to small robots.

This work was supported in part by Army RCTA , W911NF-10-2-0016

S. Dastoor and M. Cutkosky are with the Dept. of Mechanical Engineering, Stanford University, Stanford, CA 94305, USA sanjayd@stanford.edu

II. Design and Analysis

A diaphragm design was first suggested by SRI, International and subsequently used by Artificial Muscle, Inc. as the basis for the Universal Muscle Actuator (UMA). In their design, two diaphragms, both with prestrained active material, are biased out-of-plane against each other in an antagonistic configuration. Activation of a single diaphragm causes relaxation of its prestrain, inducing displacement when a load is applied perpendicular to the diaphragm.

Instead of using the diaphragm as a prime mover, one can take advantage of voltage-induced relaxation to significantly change its out-of-plane stiffness. The significant prestrain required for acrylic dielectrics translates into measurable stiffness at zero voltage. When voltage is applied, the prestrain relaxes, dropping the effective stiffness. The diaphragm concept can be seen in Figure 1.

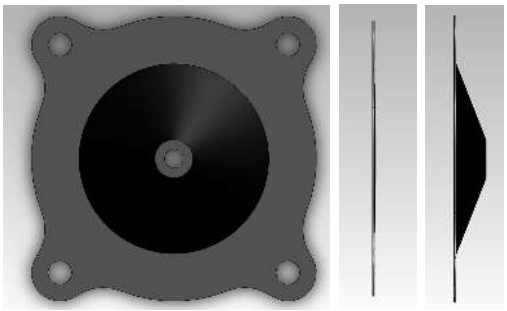

(a) (b) (c)

Fig. 1: Single layer diaphragm. (a) Front view, (b) Side view, no displacement, (c) Side view, displaced

We are interested in the relationship between the displacement of the diaphragm, x and the corresponding spring force, T_x, as well as the effect of voltage V. If we examine the stresses due to prestrain, voltage, and mechanics in an infinitesimal element of the membrane, the radial forces are scaled by cross-sectional area, which in polar coordinates has width $rd\theta$ on one side of the element and $(r + dr)d\theta$ on the other side. This causes nonlinear radial effects, such as the approximately catenoid shape of the annulus under out-of-plane deformation [18].

However, we can make some assumptions to simplify modeling of the device's behavior under small displacements. First, we assume that the out-of-plane slope of the membrane under deformation is approximately constant, forming a conical frustrum. While accurate viscoelastic models of the dielectric exist, we assume the material to be linear-elastic, since moderate displacements of the diaphragm only cause small displacements of the dielectric material. We begin by examining one cross-sectional slice of material, as shown in Figure 2.

The relationship between the tension in the prestrained film and the displacement of the film is given by

$$T = T_0 + k(L - L_0) - T_v \tag{1}$$

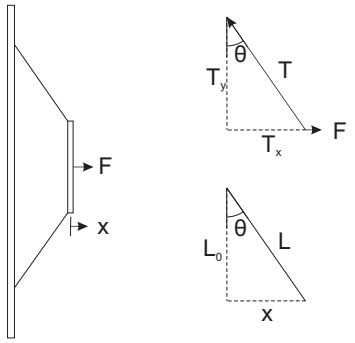

Fig. 2: Side view of single diaphragm on the left with applied force F and resulting displacement x. Radial slice on the right shows film tension T split into component forces. Summing over a symmetric diaphragm, T_y terms cancel and T_x terms equal F.

where T_0 is the tension due to prestrain, L_0 is the film length at $x = 0$, and T_v is the relaxation due to applied voltage. To calculate the relationship between the displacement of the diaphragm, x and the required force, T_x we use trigonometry to show that

$$\cos\theta = \frac{x}{L} = \frac{T_x}{T} \tag{2}$$

$$L = \sqrt{x^2 + L_0^2} \tag{3}$$

So

$$T_x = \frac{(T_0 - T_v)x}{\sqrt{x^2 + L_0^2}} + kx(1 - \frac{L_0}{\sqrt{x^2 + L_0^2}}) \tag{4}$$

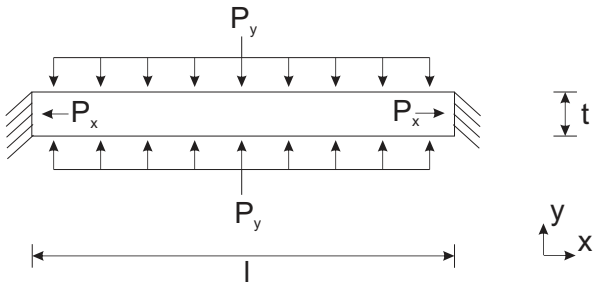

Fig. 3: Effective electrostatic pressure applied to a constrained film of unit width

The effect of voltage on the tension in the film can be modeled as in Figure 3. For a given radial slice of the frustrum membrane and an incompressible material, the slice experiences zero strain due to boundary conditions, giving us a hydrostatic pressure equivalence:

$$P_x = P_y \tag{5}$$

The effective Maxwell pressure due to an applied electric field is given [14] by

$$p = \epsilon_0 \epsilon_r E^2 = \frac{\epsilon_0 \epsilon_r V^2}{t^2} \tag{6}$$

For length l, thickness t, and width w, the voltage-induced relaxtion T_v in the film is

$$T_v = P_x t w \tag{7}$$

$$T_v = \frac{\epsilon_0 \epsilon_r V^2 w}{t} \tag{8}$$

Finally, we must include the relationship between t and x. Since radial symmetry precludes any change in w and the material is incompressible, we know that

$$t = \frac{t_0 l_0}{l} = \frac{t_0 L_0}{\sqrt{x^2 + L_0^2}} \tag{9}$$

Combining equations (4), (8), and (9), we get a relationship between T_x, x, and V:

$$T_x = (\frac{T_0 - k L_0}{\sqrt{x^2 + L_0^2}} + k - \frac{\epsilon_0 \epsilon_r V^2 w}{t_0 L_0}) x \tag{10}$$

III. Manufacturing

Actuators were based on an acrylic film, VHB 4910 (3M Corporation, USA), that was prestrained biaxially 400% x 400%. A silicone or latex film was applied over the entire non-active film area, preventing tearing and early dielectric breakthrough at the electrode edges [19]. Masks were applied and the film sprayed with conductive electrode composed of carbon black powder (Vulcan XC72R, Cabot Corporation, USA) and polydimethylsiloxane (PDMS) oil (ClearCo, USA), thinned with hexanes. Details on the process can be seen in [17]. An exploded view of the actuator is shown in Figure 4

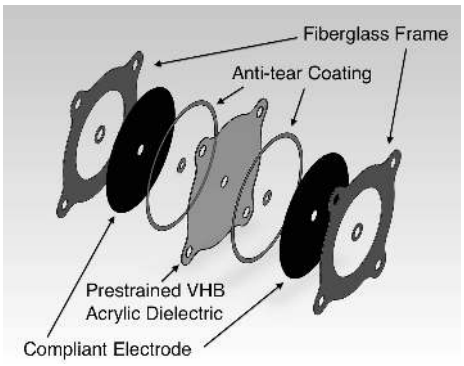

Fig. 4: Exploded view of diaphragm

Hand alignment was sufficient for the planar actuators in [17], with large actuator parts and only single layers of dielectric. When these techniques were applied to diaphragms, misalignment was frequent. As seen in Figure 5, smaller parts, free-floating elements, and multiple layers caused offsets between overlapping layers. Resulting actuators had low manufacturing yields or early failures due to high voltage arcing and stress concentrations at stiff-soft interfaces. In addition, it was noted empirically that both electrical shorts and mechanical tears almost always initiated at the electrode edges.

To address this, an alignment system was implemented for each mask and part. Templates were made from acrylic and non-stick backing layers using a laser cutter (Helix 24, Epilog, USA) to allow rapid yet precise hand placement without damaging the dielectric film. As a result, the time needed for a single actuator manufacturing run dropped to approximately 1 hour, with the volume limited only by the laser cutter bed dimensions, while the manufacturing yields improved to close to 100%.

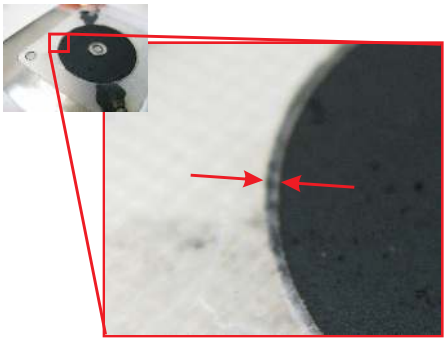

Fig. 5: Example actuator showing misalignment of fiberglass frame and compliant electrode. The distance between the arrows is approximately 800 μm.

An important advantage of the alignment system was the ability to implement small but consistent overlaps between the electrode material and the anti-tear coating. This effectively thickens the film at the mechanical interface, providing two advantages. First, this decreases stress concentrations under loading and results in fewer mechanical failures. Second, the charges on each electrode repel each other, resulting in locally higher voltages at the edges of the electrode. Increasing the film thickness at the edges reduces the electric field strength, reducing the likelihood of dielectric breakdown. The implementation of this coating layer has resulted in actuator samples with thousands of cycles of both mechanical and electrical loading without failure either during shelf storage or testing.

Design variables for a single diaphragm, besides generalized actuator parameters such as prestrain, are limited to inner and outer diameter of the active area. For a proof-of-concept test, the inner diameter was minimized without jeopardizing arcing while the outer diameter was chosen for ease of handling and testing.

IV. Experimental Results

Experimental data were collected using a muscle lever (305B, Aurora Scientific, Canada) that can prescribe either a force or length trajectory and return measured force and length. The model used in these experiments was limited to

5N of force and 20mm of displacement. A photograph of the test setup is shown in Figure 6.

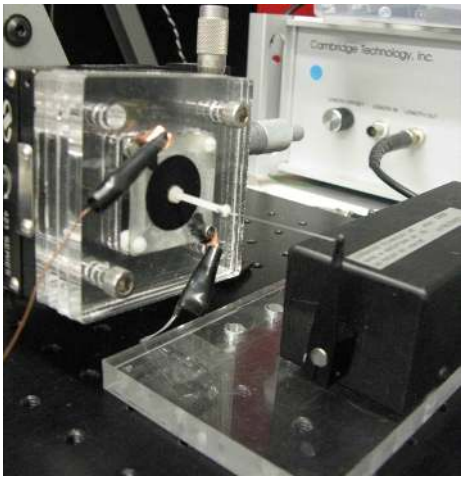

Fig. 6: Test setup with muscle lever and single layer diaphragm

Sinusoidal length trajectories were applied for five seconds. The resulting force vs length curve, known as a workloop, is commonly used in characterization of compliant biological tissue [20]. An ideal spring would yield a perfectly linear plot. Hysteresis, represented by the area inside the loop, indicates losses due to damping. As seen in the planar sample test in Figure 7, VHB 4910 has considerable viscoelastic losses, complicating modeling and constraining its application as a variable stiffness device.

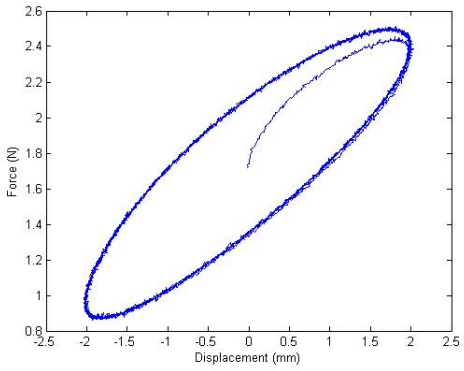

Fig. 7: Workloop test on planar sample of VHB 4910

However, the geometry of a diaphragm actuator results in a significantly more linear response, as in Figure 8. This is due in part to the low strain of the active material relative to displacement of the diaphragm. Viscoelastic losses become noticeable at higher displacements, but are still much lower than for the base VHB material.

The relationship between F, x, and V generally matches the model presented in Equation 10. Figure 9 shows force-displacement curves for different voltages. Note that for displacements above 2.5mm, viscoelastic losses, nonlinear

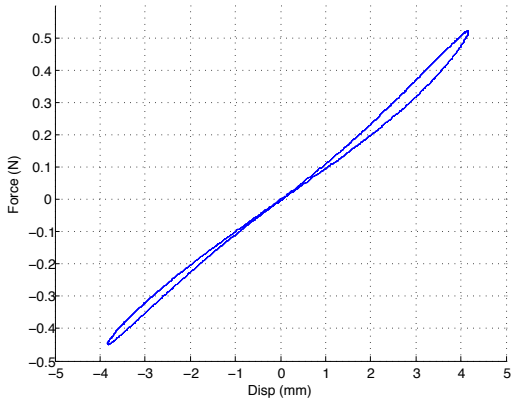

Fig. 8: Workloop test on a single diaphragm. Test was conducted at 1Hz with +/- 4mm of displacement and no applied voltage

film loading, and nonlinear voltage relaxation cause some deviation from the model.

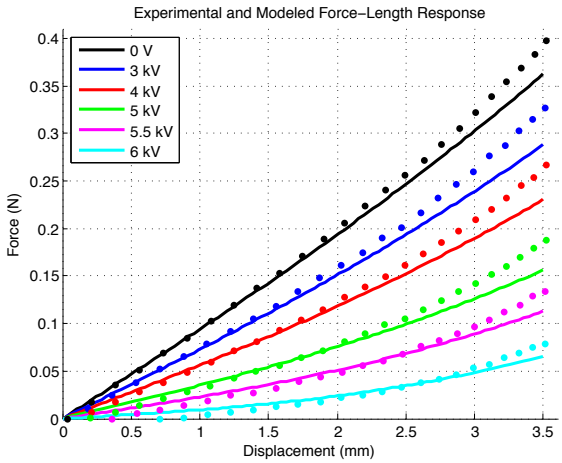

Fig. 9: Modeled vs experimental force-displacement for different applied voltages. Dotted lines are experimental, solid lines are modeled

The slope of the workloop, dF/dx, is the effective stiffness. By calculating the average stiffness over several displacement ranges and voltages, a map can be formed as in Figure 10 and Figure 11. We can see that for low frequencies, average stiffness slightly increases as displacement increases, but generally there is a 700-1000% possible change in stiffness. As frequencies increase, the viscoelastic losses at high displacements become significant, increasing the average stiffness and decreasing the change to approximately 400%. A summary of the properties of the test unit are shown in Table I.

V. Multi-unit Concept

The stiffness of a single diaphragm is limited by the stiffness of the actuator material. To scale stiffness for a given application, more than one actuator layer is necessary. One

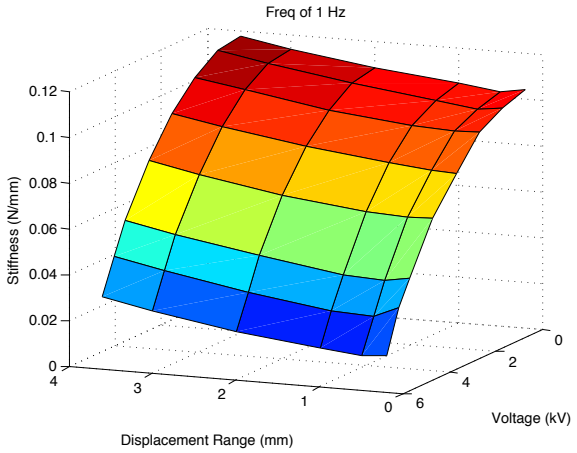

Fig. 10: Stiffness vs Voltage and Displacement Range at 1 Hz

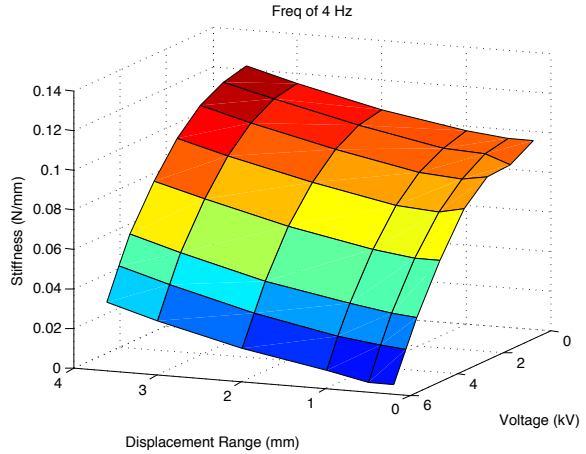

Fig. 11: Stiffness vs Voltage and Displacement Range at 4 Hz

option is the use of multiple layers in the same diaphragm unit. However, previous attempts have resulted in premature failure and low life-times, in part due to shear-induced abrasion between adjacent layers. In addition, a multi-layer diaphragm unit, due to the contact between electrodes, must have identical geometry and electrical activation across all layers.

We propose the use of single layer diaphragm units in a stacked configuration, as shown in Figure 12 and with exaggerated geometries and spacing in Figure 13. Design variables include the spacing between units (a_n), the offset between output shafts (b_n), the applied voltages (V_n), and the diameter of each unit (L_n). Each unit's force-length curve would depend on its geometry and applied voltage, while the equilibrium position would be shifted by the unit spacing and output offsets. The force-length curves, or stiffness profiles, of each unit are superimposed to give the stiffness profile of the entire stack. By manipulating the design variables, custom profiles can be constructed for a given application. Independent voltage channels for each actuator would allow

TABLE I: Test diaphragm properties

Mass (g)	1.6
Dimensions (mm)	38 x 38 x 0.7
Inner diameter (mm)	5.5
Outer diameter (mm)	25
Displacement range (mm)	8
Stiffness range over 1 mm (N/m)	15 - 102
Stiffness range over 8 mm (N/m)	32 - 117

Fig. 12: Multi-unit stack concept

even more customization during operation.

As a simple example, consider two units with $L_1 = L_2$ and $V_1 = V_2$. By varying the displacement bias before coupling them, which varies the quantity $a - b$, we can shift each diaphragm's equilibrium point along its force-length curve, as seen in Figure 14a. Lining up these equilibrium points (in a way that achieves force balance) and adding the curves yields the resultant profile, as shown in Figure 14b. Biasing and shifting a linear spring curve always yields a linear output, but, as seen in this example, a nonlinear curve can be linearized.

VI. CONCLUSIONS

We have designed, constructed, and tested an annular electroactive polymer device with variable passive compliance. It does not fall into previous categories of antagonistic or structure-controlled devices, instead relying on a combination of electric actuation and a viscoelastic load-bearing structure in a single material. This makes the device light, compact, scalable, and mechanically simple, while leveraging the inherent bandwidth and low power consumption of dielectric EAP actuators. We believe that this device is well-suited to robotic and rehabilitation systems.

Some of the known disadvantages of dielectric EAP actuators are mitigated in this approach. Failure rates will require more characterization, but empirically we have seen higher manufacturing yield rates (approaching 100%) and very low failure rates (>1000 cycles before failure) compared to earlier experiments after implementation of our aligned manufacturing techniques and the addition of the anti-tear coating. Damping losses are reduced in comparison to other geometries and, since this device is designed to part of a suspension system rather than an actuator, some damping is acceptable for most applications. Additional controllable damping can be achieved using the methods reported in [17]. High voltage requirements remain a limitation, although low current draw allows use of ultra-compact DC-DC converters.

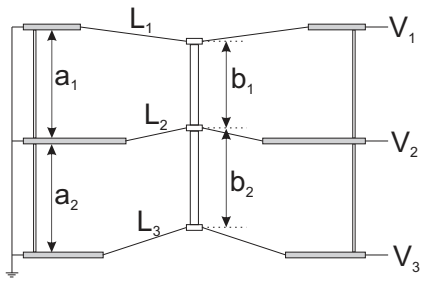

Fig. 13: Cross-section of three units.

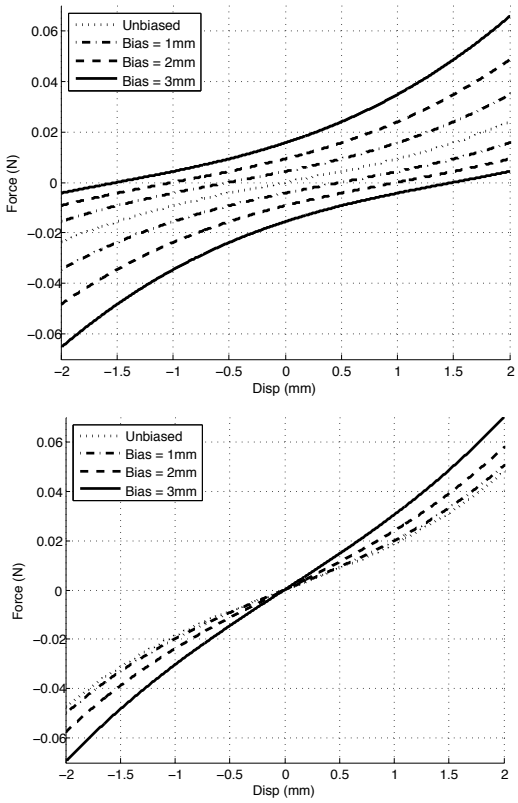

Fig. 14: Simulated stiffness profile for two unit multi-stack. (a) Individual unit profiles for varying biases. (b) Stack profile for varying biases.

Further work will focus on implementation of the multi-layer stack concept. In addition, thorough characterization of the actuator and its performance limits, especially at frequencies higher than 4 Hz, is necessary. Breakdown tests, both in terms of voltage and displacement, will be conducted. Modeling of the device at high strains will incorporate the nonlinearities of the VHB to allow use in dynamic system models. Finally, implementation of this device on a robotic platform in need of tunable compliance would validate its performance estimates and provide valuable feedback on in-situ weaknesses and strengths.

VII. ACKNOWLEDGEMENTS

The authors would like to thank Tom Libby and Bob Full at UC Berkeley for equipment use. They would also like to acknowledge support from the Bio-X program at Stanford University. This work was funded in part by the ARL RCTA, W911NF-10-2-0016.

REFERENCES

[1] S. Kim, J. Clark, and M. R. Cutkosky, "iSprawl: Design and tuning for high-speed autonomous open-loop running," *The International Journal of Robotics Research*, vol. 25, no. 9, pp. 903–912, Sep. 2006.

[2] M. H. Raibert, H. B. Brown, and M. Chepponis, "Experiments in balance with a 3D one-legged hopping machine," *The International Journal of Robotics Research*, vol. 3, no. 2, pp. 75–92, Jun. 1984.

[3] S. Kim, M. Spenko, S. Trujillo, B. Heyneman, D. Santos, and M. R. Cutkosky, "Smooth vertical surface climbing with directional adhesion," *IEEE Transactions on Robotics*, vol. 24, no. 1, pp. 65–74, 2008.

[4] A. Lussier Desbiens, A. Asbeck, and M. R. Cutkosky, "Landing, perching and taking off from vertical surfaces," *The International Journal of Robotics Research*, vol. 30, no. 3, pp. 355–370, Jan. 2011.

[5] N. Hogan, "Adaptive control of mechanical impedance by coactivation of antagonist muscles," *IEEE Transactions on Automatic Control*, vol. 29, no. 8, pp. 681–690, Aug. 1984.

[6] D. Shin, I. Sardellitti, Y. L. Park, O. Khatib, and M. Cutkosky, "Design and control of a bio-inspired human-friendly robot," *The International Journal of Robotics Research*, vol. 29, no. 5, pp. 571–584, Nov. 2009.

[7] H. Krebs, B. Volpe, M. Aisen, and N. Hogan, "Increasing productivity and quality of care: Robot-aided neuro-rehabilitation," *Journal Of Rehabilitation Research And Development*, pp. 639–652, Dec. 2000.

[8] G. A. Pratt and M. M. Williamson, "Series elastic actuators," in *Proc of Intl Conf on Intelligent Robots and Systems (IEEE-IROS)*, 1995, pp. 399–406.

[9] R. Van Ham, T. Sugar, B. Vanderborght, K. Hollander, and D. Lefeber, "Compliant actuator designs," *IEEE Robotics and Automation Magazine*, pp. 81–94, Sep. 2009.

[10] J. W. Hurst, J. E. Chestnutt, and A. Rizzi, "Design and philosophy of the BiMASC, a highly dynamic biped," in *Proc of Intl Conf on Robotics and Automation (IEEE-ICRA)*, Apr. 2007, pp. 1863–1868.

[11] K. Galloway, J. Clark, and D. Koditschek, "Design of a tunable stiffness composite leg for dynamic locomotion," in *Proc of Intl Design Engineering Technical Conf (ASME-IDETC/CIE)*, 2009.

[12] K. W. Hollander, T. G. Sugar, and D. E. Herring, "Adjustable robotic tendon using a Jack Spring," in *Proc of Intl Conf on Rehabilitation Robotics (IEEE-ICORR)*, 2005, pp. 113–118.

[13] K. W. Hollander and T. G. Sugar, "Concepts for compliant actuation in wearable robotic systems," in *Proc of the US-Korea Conf on Science, Technology, and Entrepreneurship*, vol. 128, 2004, pp. 644–650.

[14] R. Pelrine, R. Kornbluh, Q. Pei, and J. Joseph, "High-speed electrically actuated elastomers with strain greater than 100%," *Science*, vol. 287, no. 5454, pp. 836–839, Feb. 2000.

[15] R. Pelrine, "Variable stiffness mode: Devices and applications," in *Dielectric Elastomers as Electromechanical Transducers*, F. Carpi, D. De Rossi, R. Kornbluh, R. Pelrine, and P. Sommer-Larsen, Eds. Elsevier, 2008, ch. 14.

[16] R. Pelrine and R. Kornbluh, "Variable-stiffness-mode dielectric elastomer devices," *Advances in Science and Technology*, vol. 61, pp. 192–201, 2008.

[17] S. Dastoor and M. R. Cutkosky, "Variable impedance due to electromechanical coupling in electroactive polymer actuators," in *Proc of Intl Conf on Intelligent Robots and Systems (IEEE-IROS)*, 2011.

[18] W. Yu and D. G. Karr, "Symmetrical solutions for edge-loaded annular elastic membranes," *Journal of Applied Mechanics*, vol. 76, no. 3, p. 031010, 2009.

[19] R. Pelrine, R. Kornbluh, H. Prahlad, S. Sharma, B. Chavez, D. Czyzyk, A. Wong-Foy, and S. Stanford, "Tear resistant electroactive polymer transducers," U.S. Patent 7,804,227, 2010.

[20] R. K. Josephson, "Mechanical power output from striated muscle during cyclic contraction," *Journal of Experimental Biology*, vol. 114, pp. 493–512, 1985.